RESEARCH PAPER

Synergistic Impact of Mechanical Alloying Duration and Spark Plasma Sintering Temperature on Microstructure and Properties of CoCrFeNiMn High-Entropy Alloys

Saeed Jafari Varjoshani[1], Alireza Hajialimohammadi[1,*], Masoud Mahmoodi[1], Rashi Tyagi[2]

* *ahajiali@semnan.ac.ir*

[1] Faculty of Mechanical Engineering, Semnan University, Semnan, Iran
[2] Department of Mechanical Engineering Galgotias University, Greater noida, India

Received: June 2025 **Revised: December 2025** **Accepted: March 2026**
DOI: 10.22068/ijmse.4140

Abstract: *This study successfully synthesized the CoCrFeNiMn high-entropy alloy (HEA) using a two-step powder metallurgy approach: mechanical alloying (MA) followed by spark plasma sintering (SPS). The research investigated the effects of processing parameters, specifically MA duration and SPS temperature, on the alloy's microstructure, densification, and mechanical properties. X-ray diffraction (XRD) analysis after 25 hours of MA (ball-to-powder ratio of 10:1) confirmed the formation of a single-phase face-centered cubic (FCC) solid solution. Scanning electron microscopy (SEM) images revealed significant powder particle refinement, with average particle sizes decreasing from initial micrometers to sub-micrometer ranges. The alloyed powders were then consolidated via SPS at temperatures of 800°C, 900°C, and 1000°C (40 MPa, 10 min in argon). Detailed analysis of the sintered samples showed relative densities ranging from 95.78% to 96.77%, with the highest density (96.77%) achieved at 1000°C. Vickers microhardness measurements exhibited a peak hardness of 446 HV at 900°C, with a decrease to 420 HV at 1000°C, primarily due to grain growth. This research establishes the combined MA and SPS approach as effective for producing high-density, high-hardness HEAs, underscoring the critical role of processing parameters in tailoring their final properties.*

Keywords: *High-Entropy Alloys (HEAs), Mechanical alloying, Spark Plasma Sintering (SPS), Microstructural refinement, Vickers hardness.*

1. INTRODUCTION

High-entropy alloys (HEAs) have garnered significant attention in materials science due to their unique compositional paradigm, which incorporates at least five principal elements in near-equiatomic concentrations (typically 5–35 at. %) [1–3]. This departure from conventional alloy design, typically centered on one dominant element, facilitates the formation of simple solid solution phases stabilized by high configurational entropy.

This fundamental characteristic often endows HEAs with an extraordinary suite of properties, including exceptional mechanical strength, notable ductility, superior corrosion and wear resistance, and remarkable thermal stability [4−6]. Among the extensive catalog of HEA systems, the equiatomic CoCrFeMnNi alloy, commonly known as the Cantor alloy, stands as a prototypical and extensively studied face-centered cubic (FCC) solid solution [7]. First reported by Cantor et al., this alloy exhibits a compelling balance of high strength and ductility, retains excellent fracture toughness even at cryogenic temperatures, and demonstrates impressive microstructural stability, making it a prime candidate for demanding applications in aerospace, automotive, and energy sectors [8-13]. The superior properties of HEAs are attributed to a synergistic interplay of core effects, including severe lattice distortion, sluggish diffusion kinetics, the so-called "cocktail effect," and the high-entropy stabilization of solid solutions, which collectively impede dislocation motion and enhance mechanical performance [14-16]. Beyond bulk properties, HEAs also show immense promise as protective coatings applied via thermal spray or plasma techniques, offering enhanced resistance to wear, corrosion, and high-temperature oxidation [17-20]. Despite their immense potential, the fabrication of homogeneous and fine-grained HEAs via conventional melting and casting techniques, such as vacuum arc melting or induction melting, faces inherent challenges. These methods are often prone to issues like elemental segregation, dendritic solidification, evaporation of volatile constituents (e.g., Mn), and the formation of coarse-grained or inhomogeneous microstructures due to prolonged high-temperature exposure [21-23]. Achieving the desired microstructural refinement and chemical homogeneity frequently necessitates

[Downloaded from pga.iust.ac.ir on 2026-10-19]

[DOI: 10.22068/ijmse.4140]

subsequent, energy-intensive thermo-mechanical processing steps, such as severe plastic deformation followed by annealing, which adds complexity and cost [24-26].

Powder metallurgy (PM) routes, particularly the synergistic combination of mechanical alloying (MA) and spark plasma sintering (SPS), have emerged as a highly effective alternative to circumvent these limitations [27-30]. MA, a high-energy ball milling process, mechanically alloys elemental powders at room temperature, facilitating atomic-level mixing, refining crystallite sizes to the nanoscale, and forming homogeneous solid solutions while minimizing evaporation losses [31-33].

Subsequent consolidation via SPS utilizes pulsed direct current and uniaxial pressure to achieve near-full density at significantly lower temperatures and shorter dwell times compared to conventional sintering. This rapid process effectively suppresses excessive grain growth, thereby preserving the refined microstructures attained during MA [27, 29, 30].

For instance, nanostructured Cantor alloys processed via MA+SPS have demonstrated ultimate tensile strengths exceeding 1200 MPa, nearly double that of their as-cast counterparts, while maintaining appreciable ductility [34]. These results underscore the critical role of optimized PM processing in tailoring microstructures for enhanced mechanical performance.

While the individual effects of MA or SPS parameters on HEA properties have been explored in prior studies [35-40], a comprehensive understanding of their synergistic interplay remains less charted. Specifically, a systematic investigation correlating specific MA durations with subsequent SPS temperatures for the CoCrFeNiMn system is needed to delineate their combined impact on phase stability, densification kinetics, microstructural evolution (including grain size and chemical homogeneity), and the resulting mechanical properties.

Therefore, this study aims to systematically investigate the synergistic influence of mechanical alloying duration (5, 10, 15, 20, and 25 hours) and spark plasma sintering temperature (800°C, 900°C, and 1000°C) on the synthesis, microstructure, and properties of equiatomic CoCrFeNiMn HEAs. The novelty of this work lies in its quantitative and correlated approach, which meticulously links specific processing steps to final material outcomes. Using a suite of characterization techniques including X-ray diffraction (XRD), scanning electron microscopy with energy-dispersive spectroscopy (SEM/EDS), density measurements, and Vickers microhardness testing, we elucidate the processing-structure-property relationships. The overarching goal is to identify optimal processing windows that balance high densification with microstructural refinement, thereby establishing robust guidelines for fabricating high-performance CoCrFeNiMn HEAs suitable for advanced engineering applications.

2. EXPERIMENTAL PROCEDURES

2.1. Preparation of Elemental Powders

In this study, equiatomic CoCrFeNiMn HEA powder was synthesized via mechanical alloying. High-purity (>99%) elemental powders of Cobalt (Co), Chromium (Cr), Iron (Fe), Manganese (Mn), and Nickel (Ni) were used as starting materials. The powders were supplied by Sigma-Aldrich, with initial particle sizes ranging between 1-5 µm. To achieve the target equiatomic composition, the required weight of each element was calculated based on its atomic percentage (Table 1). The powders were precisely weighed using a high-accuracy analytical balance (Sartorius, ±0.1 mg) to maintain a stoichiometric ratio of 20 at.% for each element.

Prior to mechanical alloying, the weighed powders were pre-mixed in a turbula mixer (Willy A. Bachofen, Switzerland) for 30 minutes to ensure initial homogeneity and minimize segregation, thereby enhancing the efficiency of the subsequent high-energy milling process.

Table 1. Specification of starting elemental powders

Element	Atomic %	Purity (%)	Particle size (µm)	Weight % in blend
Co	20	>99	1-5	21.02
Cr	20	>99	1-5	18.54
Ni	20	>99	1-5	20.94
Mn	20	>99	1-5	19.58
Fe	20	>99	1-5	19.92

[Downloaded from pga.iust.ac.ir on 2026-10-19]

[DOI: 10.22068/ijmse.4140]

2.2. Mechanical Alloying

Mechanical alloying was performed in a high-energy planetary ball mill (Retsch PM 400, Germany) (Figure 1) using zirconia vials and balls (10 mm diameter) to minimize iron contamination. A constant ball-to-powder weight ratio (BPR) of 10:1 was maintained, which is known to provide an optimal balance between impact energy and milling efficiency for HEA synthesis [28, 29]. The milling was conducted at a rotational speed of 250 rpm. To prevent excessive cold welding and particle agglomeration, 1 wt.% of ethanol was added as a process control agent (PCA). The total milling process was divided into five distinct durations: 5, 10, 15, 20, and 25 hours. At each interval, a small amount of powder was extracted under an argon atmosphere for intermediate characterization, allowing the monitoring of phase evolution and microstructural changes.

2.3. Spark Plasma Sintering

Consolidation of the 25-hour milled powder, identified as fully alloyed, was carried out using a spark plasma sintering system (SPS-211Lx, Fuji Electronic Industrial Co., Japan) (Figure 1). Approximately 5 grams of powder were loaded into a cylindrical graphite die with an inner diameter of 20 mm. The sintering process was conducted under a dynamic vacuum (≤ 6 Pa). Three different peak temperatures were investigated: 800°C, 900°C, and 1000°C. All samples were heated at a rate of 50°C/min under a constant uniaxial pressure of 40 MPa, held at the peak temperature for 10 minutes, and subsequently furnace-cooled to room temperature under an argon flow. The use of rapid heating and simultaneous pressure application in SPS is crucial for achieving high density while limiting grain growth [27, 30].

The density of the sintered pellets was measured using the Archimedes' principle (ASTM B962) with deionized water as the immersion medium. The theoretical density of the equiatomic CoCrFeNiMn alloy (approximately 7.98 g/cm³) was used as a reference to calculate the relative density and porosity.

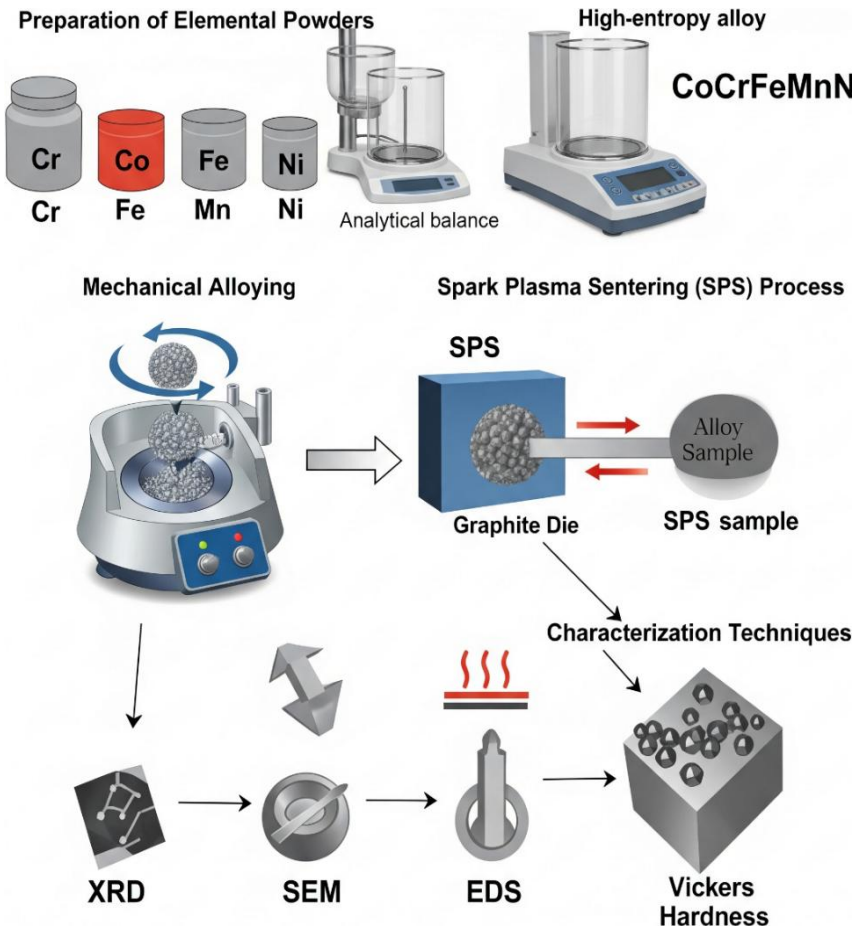

Fig. 1. Mechanical alloying in a high-energy planetary ball mill operating at 250 rpm and the SPS apparatus equipped with graphite dies to ensure uniform heating

[Downloaded from pga.iust.ac.ir on 2026-10-19]

[DOI: 10.22068/ijmse.4140]

2.4. Microstructural Characterization

The phase composition and structural parameters of the powders and sintered samples were characterized as follows:

Phase identification was performed using a Bruker D8 Advance diffractometer with Cu-Kα radiation (λ= 1.5406 Å, 40 kV, 30 mA). Scans were recorded in the 2θ range of 20–100° with a step size of 0.02° and a scan speed of 2°/min. The obtained patterns were analyzed using DIFFRAC.EVA software. Crystallite size and lattice microstrain were quantitatively estimated from the peak broadening using the Williamson-Hall (W-H) method, providing insights into the refinement induced by mechanical alloying [31].

The morphology of the milled powders and the microstructure of the sintered and polished samples were examined using a field-emission scanning electron microscope (FE-SEM, TESCAN MIRA3). Secondary electron (SE) and backscattered electron (BSE) imaging were performed at an accelerating voltage of 20 kV. Chemical homogeneity and elemental distribution were assessed via EDS mapping and point analysis using an Oxford Instruments X-Max detector. Grain size measurements of the sintered samples were performed by analyzing SEM micrographs using the linear intercept method (according to ASTM E112) on at least 200 grains per condition.

2.5. Mechanical Property Testing

The mechanical hardness of the polished sintered samples was evaluated using a Vickers microhardness tester (Wolpert Wilson 432 SVD) with a load of 0.5 kgf (4.903 N) and a dwell time of 15 seconds. To ensure statistical reliability and account for potential microstructural heterogeneity, a minimum of 10 indentations were made at randomly selected locations on each sample, and the average value along with the standard deviation is reported.

3. RESULTS AND DISCUSSION

3.1. Microstructural Evolution During Mechanical Alloying

The microstructural evolution during the MA process, a critical solid-state synthesis route, was systematically investigated using XRD, SEM, and EDS. Our comprehensive analysis reveals a clear, time-dependent progression from a blend of distinct elemental powders to a chemically homogeneous, nanocrystalline, single-phase face-centered cubic (FCC) high-entropy alloy.

The phase transformation was meticulously tracked via XRD patterns collected after 5, 10, 15, 20, and 25 hours of milling (Figure 2). The initial pattern (5 h) displays sharp, well-defined diffraction peaks corresponding to the crystalline structures of the pure elements: the FCC phases of Nickel (Ni), Cobalt (Co), and Iron (Fe), alongside the body-centered cubic (BCC) phase of Chromium (Cr). The most immediate and pronounced effect of milling is the significant broadening and decrease in intensity of all diffraction peaks as time increases. This phenomenon is a direct consequence of the severe plastic deformation imparted by high-energy ball collisions, which introduces a high density of lattice defects (dislocations, vacancies) and progressively refines the crystalline domains [31, 32].

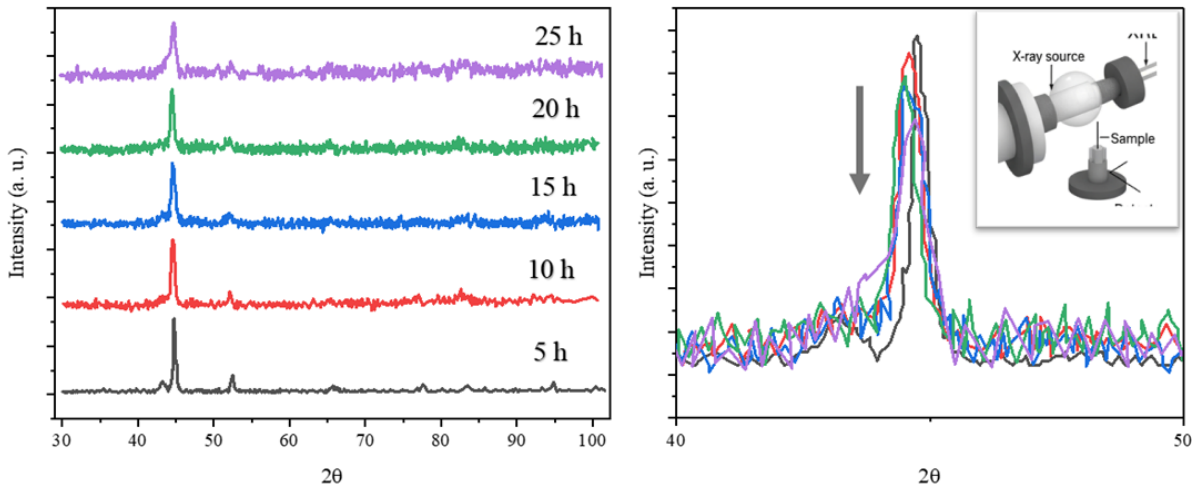

Fig. 2. XRD patterns of the CoCrFeNiMn powder blend after 5, 10, 15, 20, and 25 hours of mechanical alloying, showing the dissolution of elemental peaks and formation of a single FCC solid solution phase

[Downloaded from pga.iust.ac.ir on 2026-10-19]

[DOI: 10.22068/ijmse.4140]

Between 10 and 15 hours, a critical transition occurs: the individual elemental peaks begin to overlap and merge into a broad, asymmetric profile. This indicates the onset of extensive atomic-level interdiffusion, where solute atoms (e.g., Cr with its BCC structure) dissolve into the dominant FCC matrices, leading to the formation of a supersaturated solid solution. After 20 hours of milling, the pattern converges into a single, very broad diffraction halo, signifying the near-complete dissolution of elemental phases into an amorphous or extremely nanocrystalline state. The final stage, achieved at 25 hours, is marked by the emergence of a single, smooth, and broadened FCC peak, unequivocally confirming the synthesis of a single-phase CoCrFeNiMn HEA solid solution. The complete absence of any residual elemental peaks underscores the efficacy of MA in overcoming thermodynamic barriers and achieving full chemical homogeneity, a finding that aligns with the seminal work on equiatomic multicomponent alloys [7].

To quantify the extreme microstructural refinement, we applied the Williamson-Hall (W-H) analysis to deconvolute the effects of crystallite size and lattice strain on XRD peak broadening (Table 2). The results are striking: the average crystallite size is refined from 45 ± 5 nm after just 5 hours to 12 ± 2 nm after 25 hours, a reduction of over 70%. Concurrently, the root-mean-square (RMS) lattice strain escalates from a minimal 0.15% to 0.82%. This inverse relationship highlights the core mechanism of MA: intense deformation simultaneously fractures crystalline domains and stores energy in the lattice through defects. This nanocrystalline, highly strained state is not merely a structural curiosity; it is a foundational precursor for superior mechanical properties. The ultra-fine crystallites provide a massive increase in grain boundary area, which acts as potent barriers to dislocation motion (Hall-Petch strengthening), while the high dislocation density associated with lattice strain contributes directly to dislocation hardening [38, 39].

Furthermore, the stabilization of this single-phase FCC structure, despite the presence of multiple elements with varying crystal structures, is powerfully driven by the high configurational entropy of the equiatomic composition, which thermodynamically favors disordered solid solutions over intermetallic compounds [1, 2, 36].

The XRD findings are powerfully complemented by SEM analysis of powder morphology (Figure 3). The initial blended powder consists of course, irregularly shaped particles ranging from 1 to 50 µm, reflecting the different characteristics of the constituent metals. As milling commences, the powder undergoes a dynamic and cyclic process of cold welding, fracture, and re-welding [28, 29]. By 10 hours, the particles become more equiaxed but form large, layered agglomerates due to cold welding. Continued milling (20-25 h) increasingly dominates the fracturing stage, breaking down these agglomerates. The final powder after 25 hours (Figure 3) exhibits a remarkably homogeneous morphology, comprised of fine, equiaxed particles predominantly in the sub-micrometer to a few micrometer range. This refined and uniform particle size distribution is crucial for the subsequent sintering stage, as it ensures uniform packing density and intimate interparticle contact, which are vital for achieving high densification during SPS.

The ultimate test of alloying success is chemical homogeneity at the micro-scale. EDS elemental mapping performed on the 25-hour milled powder (Figure 4) provides definitive evidence. The maps for Co, Cr, Fe, Mn, and Ni show a perfectly uniform, overlapping distribution of all five elements across the scanned area. No regions enriched in a single element or indicative of unalloyed cores are detectable. Quantitative point analysis at numerous random locations consistently yielded compositions within 1-2 at.% of the ideal 20 at.% for each element. This confirms that mechanical alloying has successfully facilitated atomic-scale diffusion, achieving a homogeneous, equiatomic solid solution powder.

Table 2. Crystallite size and lattice strain of CoCrFeNiMn powders calculated via Williamson-Hall analysis as a function of mechanical alloying time

Milling time (h)	Crystallite size (nm)	Lattice strain (%)
5	45 ± 5	0.15 ± 0.02
10	32 ± 4	0.31 ± 0.03
15	25 ± 3	0.52 ± 0.04
20	18 ± 2	0.68 ± 0.05
25	12 ± 2	0.82 ± 0.06

[Downloaded from pga.iust.ac.ir on 2026-10-19]

[DOI: 10.22068/ijmse.4140]

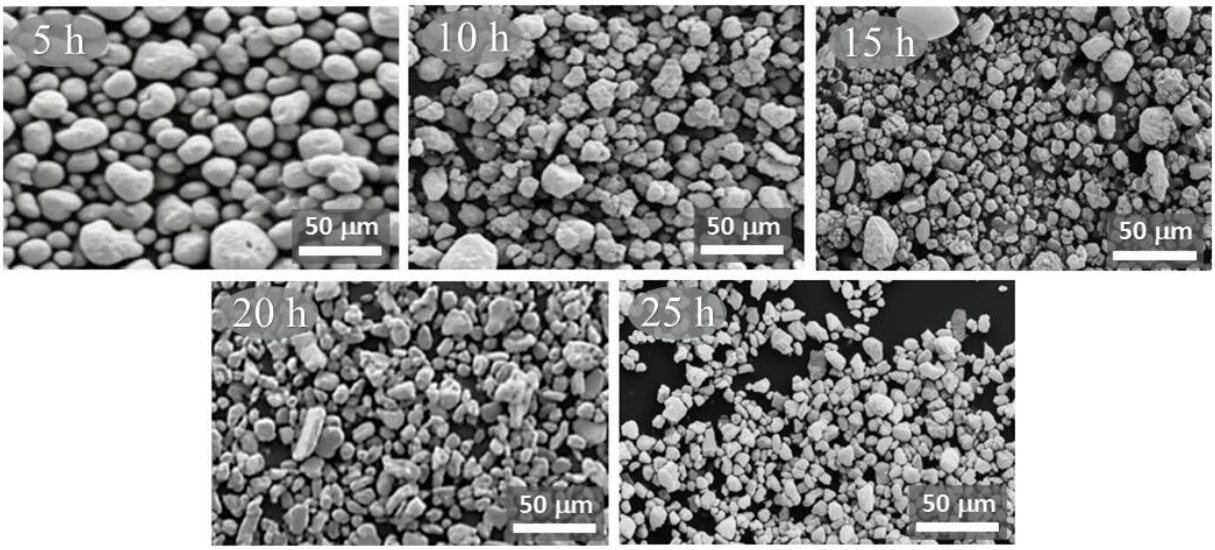

Fig. 3. SEM micrographs (secondary electron mode) illustrating the morphological evolution of powders of mechanical alloying, showing progressive refinement and homogenization

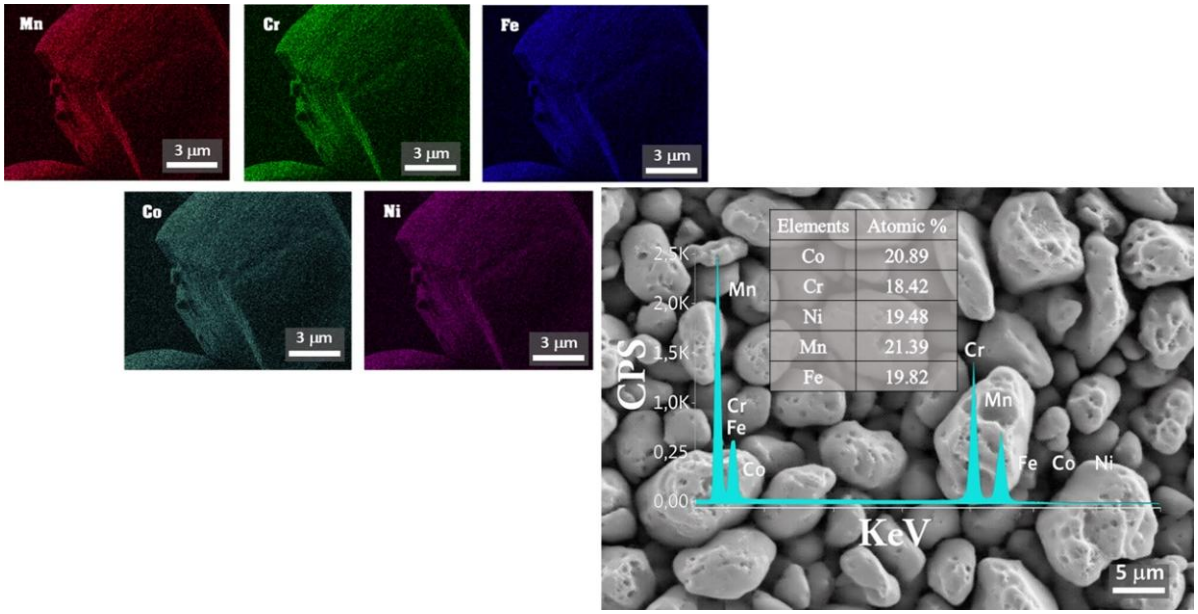

Fig. 4. EDS analysis of the powders after MA

This result highlights a seminal advantage of the MA process: it enables the synthesis of complex, multi-component alloys with excellent chemical uniformity entirely in the solid state and at near-ambient temperatures. This circumvents significant challenges inherent to liquid-state processing, such as the evaporation of volatile elements like Manganese (Mn) and macro-segregation due to differing liquidus temperatures and densities, which are commonly reported in vacuum arc melting of HEAs [21, 22, 35, 37]. The chemically homogeneous, nanocrystalline powder produced here forms an ideal precursor for consolidation, setting the stage for investigating the impact of sintering parameters on developing the final bulk microstructure and properties.

3.2. Effect of Sintering on Densification, Microstructure, and Mechanical Characteristics

The consolidation of the nanocrystalline, single-phase CoCrFeNiMn powder, synthesized via 25 hours of mechanical alloying, was achieved through SPS at three distinct temperatures: 800°C, 900°C, and 1000°C. This section investigates the critical interplay between the SPS temperature and the resulting densification behavior, micro-

[Downloaded from pga.iust.ac.ir on 2026-10-19]

[DOI: 10.22068/ijmse.4140]

structural evolution, and final mechanical performance, identifying the optimal processing window for this HEA system.

The effectiveness of the SPS consolidation process was quantitatively assessed by measuring the relative density of the sintered pellets. As graphically summarized in Figure 5, the relative density exhibits a pronounced and systematic increase with sintering temperature. It rises from 95.78 ± 0.15% at 800°C to 96.45 ± 0.12% at 900°C, culminating at the maximum value of 96.77 ± 0.10% at 1000°C. This positive correlation is a direct consequence of the fundamental SPS mechanisms activated at higher temperatures. The combination of pulsed direct current and uniaxial pressure generates localized Joule heating at particle contacts, enhances surface diffusion, and promotes plastic yielding. At elevated temperatures, these effects are amplified: atomic mobility increases dramatically, facilitating the elimination of residual pores through diffusion-controlled mechanisms like grain boundary diffusion and volume diffusion. Furthermore, the applied pressure (40 MPa) becomes more effective in driving particle rearrangement and plastic deformation, leading to improved interparticle bonding and pore closure [27, 30]. The most significant densification rate is observed between 800°C and 900°C, where a ~0.7% relative density gain is achieved. Conversely, the increment from 900°C to 1000°C is only ~0.3%, indicating that the densification process is nearing completion and approaching the theoretical limit, with remaining porosity becoming increasingly difficult to remove.

The mechanical integrity of the sintered compacts was evaluated using Vickers microhardness testing. Contrary to the monotonic increase in density, the hardness profile reveals a distinct optimum (Figure 5). Hardness escalates substantially from 398 ± 12 HV at 800°C to a peak of 446 ± 15 HV at 900°C, representing a 12% improvement. This is followed by an unexpected decline to 420 ± 14 HV at 1000°C, despite this condition yielding the highest density. This non-monotonic trend is a clear signature of competing microstructural phenomena, densification versus grain growth, governed by sintering temperature.

The observed peak hardness at 900°C is attributed to the synergistic achievement of two key objectives. First, the high relative density (~96.5%) attained at this temperature signifies a drastic reduction in porosity.

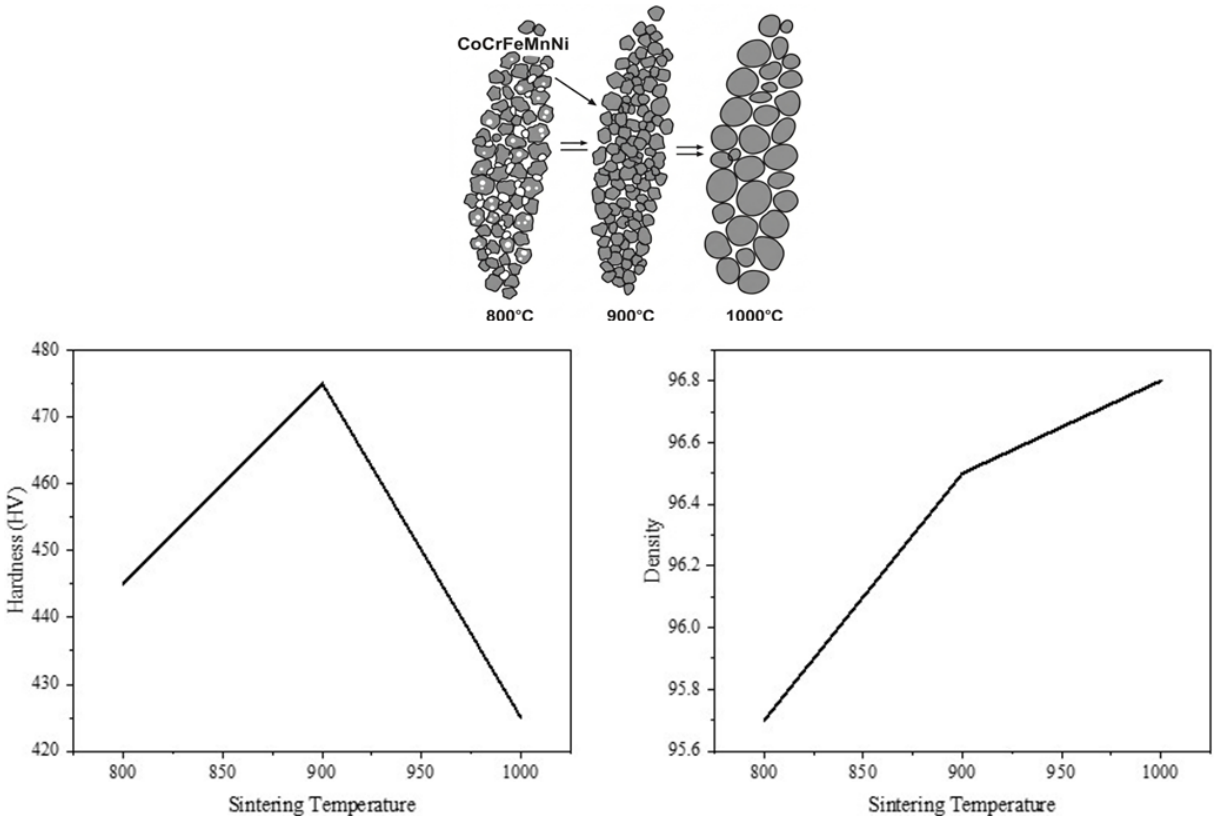

Fig. 5. Relative density and Vickers microhardness of CoCrFeNiMn HEA samples consolidated via SPS at 800°C, 900°C, and 1000°C (40 MPa, 10 min hold)

[Downloaded from pga.iust.ac.ir on 2026-10-19]

[DOI: 10.22068/ijmse.4140]

Pores are critical stress concentrators that initiate cracking and provide easy paths for crack propagation; their minimization is paramount for enhancing mechanical strength and hardness [39]. Second, the SPS process, with its characteristic rapid heating rates (50°C/min) and short isothermal holds (10 minutes), provides a limited time-at-temperature. At 900°C, this thermal budget is sufficient to activate diffusion for pore removal but is largely insufficient to drive extensive grain boundary migration. Consequently, a significant fraction of the refined, nanocrystalline structure inherited from the mechanically alloyed powder is preserved. This retention of a fine-grained microstructure is crucial, as grain boundaries act as potent barriers to dislocation motion. The combined effect of high density (fewer defects) and a fine grain size (more barriers) maximize the material's resistance to plastic deformation, resulting in peak hardness.

The decrease in hardness at 1000°C, even with the highest density, is a classic demonstration of a materials science trade-off. While the marginal density gain from 96.45% to 96.77% offers a negligible strengthening contribution, the additional 100°C of thermal energy profoundly impacts the microstructure. The driving force for grain growth is exponentially dependent on temperature. At 1000°C, this force becomes dominant, overcoming the kinetic limitations imposed by the short SPS cycle. Significant grain coarsening occurs, as confirmed by microstructural analysis. This growth directly weakens the material via the well-established Hall-Petch relationship $\sigma_y = \sigma_0 + k_y d^{-1/2}$, where yield strength ($\sigma_y$) and, by strong correlation, hardness, are inversely proportional to the square root of the grain size (d) [38, 39]. Larger grains mean fewer grain boundaries per unit volume, offering less resistance to dislocation glide and pile-up. In this regime, the detrimental softening effect induced by grain coarsening overwhelmingly surpasses the minuscule benefit from further pore elimination. This aligns with established SPS literature, which cautions that exceeding an optimal temperature window, while beneficial for density, often triggers deleterious microstructural coarsening that degrades mechanical properties [32].

Therefore, 900°C is unequivocally identified as the optimal SPS temperature for consolidating the mechanically alloyed CoCrFeNiMn HEA under the applied pressure of 40 MPa and a 10-minute hold. This parameter set successfully strikes a critical balance: it utilizes sufficient thermal energy to achieve near-full densification and robust interparticle bonding, while simultaneously leveraging the intrinsic rapidity of SPS to suppress the thermally activated grain growth that would otherwise erase the nanocrystalline advantages of the precursor powder. The success of this optimized MA-SPS route is underscored by the achieved hardness value of ~446 HV. This represents more than a twofold increase compared to the typical hardness of as-cast, coarse-grained Cantor alloy (~200 HV) [7, 23]. This dramatic enhancement validates the core premise of this study: the synergistic combination of mechanical alloying for nano-crystalline powder synthesis and carefully optimized spark plasma sintering for consolidation is a highly effective strategy for fabricating bulk high-entropy alloys with superior strength and hardness, enabled by precise microstructural control.

4. CONCLUSIONS

This study successfully demonstrates the effectiveness of a two-step powder metallurgy route, combining MA and SPS, for synthesizing bulk CoCrFeNiMn HEAs. A systematic investigation was conducted to elucidate the individual and synergistic influences of MA duration and SPS temperature on phase formation, densification, microstructure, and mechanical hardness.

The key findings are as follows: X-ray diffraction analysis confirmed that a homogeneous, single-phase FCC solid solution formed after 25 hours of MA. Williamson-Hall analysis quantified the progressive refinement, showing a decrease in crystallite size from ~45 nm (5 h) to ~12 nm (25 h) alongside a significant increase in lattice strain (from 0.15% to 0.82%). SEM and EDS analyses corroborated the formation of chemically homogeneous powder with sub-micrometer particle morphology. The SPS process effectively consolidated the alloyed powders, achieving high relative densities (>95.7%). Density increased with sintering temperature, reaching a maximum of 96.77% at 1000°C. Mechanical property evaluation revealed a non-monotonic trend in Vickers microhardness with SPS temperature. A peak hardness of 446 HV was achieved at 900°C, compared to 398 HV at 800°C and 420 HV at 1000°C. The results identify 900°C as the optimal SPS temperature under the applied conditions (40 MPa, 10 min).

[Downloaded from pga.iust.ac.ir on 2026-10-19]

[DOI: 10.22068/ijmse.4140]

This temperature represents a critical balance, maximizing densification to ~96.5% while minimizing the thermal driving force for grain growth. The subsequent decrease in hardness at 1000°C, despite the highest density, is attributed to the dominant softening effect of grain coarsening, which outweighs the marginal benefit of further pore elimination. In conclusion, this work underscores that precise control over both MA duration and SPS temperature is paramount for tailoring the microstructure and properties of CoCrFeNiMn HEAs. The established MA-SPS protocol provides a scalable and efficient pathway for manufacturing high-performance HEAs with enhanced hardness, offering clear guidelines for optimizing their processing-structure-property relationships for potential applications in demanding engineering fields.

REFERENCES

[1] Yeh, J. W., Chen, S. K., Lin, S. J., Gan, J. H., Chin, T. S., Shun, T. T., Chang, C. H. (2004). Nanostructured high-entropy alloys with multi-principal elements: Novel alloy design concepts and outcomes. Advanced Engineering Materials, 6(1-2), 1-11.

[2] Cantor, B., Chang, I. T. H., Knight, P., & Vincent, A. J. B. (2004). Microstructural development in equiatomic multicomponent alloys. Materials Science and Engineering: A, 375-377, 213-218.

[3] Zhang, Y., Zhou, Y. J., Cao, L. P., Chen, X., & Liu, C. T. (2008). Solid-solution phase formation rule for high-entropy alloys. Progress in Materials Science, 53(8), 1159-1222.

[4] Miracle, D. B., & Miller, O. N. (2014). High-entropy alloys: A new frontier for powder metallurgy. Powder Metallurgy, 57(3), 195-200.

[5] Senkov, O. N., Wilks, G. B., Miracle, D. B., Cantwell, J. D., & Vanfleet, T. R. (2010). Refractory high-entropy alloys. Materials Science and Engineering: A, 527(12), 3507-3518.

[6] Gao, M. C., Liaw, P. K., & Zhang, Y. (Eds.). (2016). High-entropy alloys: Fundamentals and applications. Springer.

[7] Cantor, B., Chang, I. T. H., Knight, P., & Vincent, A. J. B. (2004). Microstructural development in equiatomic multicomponent alloys. Materials Science and Engineering: A, 375-377, 213-218.

[8] Otto, F., Dlouhý, A., Somsen, K. H., Bei, W., Joo, G. F., & Eggeler, G. (2013). The influences of temperature and strain rate on the mechanical properties of the CrMnFeCoNi high-entropy alloy. Materials Science and Engineering: A, 560, 239-247.

[9] Gludovatz, B., Hohenwarter, A., Catoor, D., Chang, E. H., George, E. P., & Ritchie, R. O. (2014). A fracture-resistant high-entropy alloy for cryogenic applications. Science, 345(6203), 1153-1158.

[10] Laplanche, G., Steurer, W., Cornelius, D., & George, E. P. (2015). Microstructure and mechanical properties of the CrMnFeCoNi high-entropy alloy at cryogenic temperatures. Acta Materialia, 90, 356-362.

[11] George, E. P., Raabe, D., & Ritchie, R. O. (2019). High-entropy alloys. Nature Reviews Materials, 4(8), 515-528.

[12] Zhang, Y., & Kou, S. (2020). High-entropy alloys: A review of phase formation and mechanical properties. Journal of Materials Science & Technology, 41, 1-21.

[13] Rogal, L., Köster, P., Freudenberger, R., Springer, H., & Raabe, D. (2022). High-entropy alloys for aerospace applications. Materialia, 23, 101416.

[14] Miracle, D. B., & Senkov, O. N. (2017). A critical review of high entropy alloys and related concepts. Acta Materialia, 122, 448-511.

[15] Sheng, H. W., Ma, E., & Liu, Y. (2019). The intrinsic strengthening mechanisms in high-entropy alloys. Progress in Materials Science, 106, 100582.

[16] Singh, S., & Jou, H. (2021). Lattice distortion in high-entropy alloys: A critical review. Materials Today Communications, 26, 101968.

[17] Chou, Y. L., Yeh, J. W., & Shih, Y. H. (2010). High-entropy alloy coatings for wear and corrosion resistance. Surface and Coatings Technology, 204(12-13), 2269-2274.

[18] Li, S., Zhang, Y., & Liaw, P. K. (2017). Corrosion and wear behavior of high-entropy alloys: A review. Journal of Materials Research, 32(21), 3925-3944.

[19] Lu, Y., Gao, X., & Zhang, Y. (2017). Oxidation and corrosion resistance of high-entropy alloys: A review. Corrosion Science, 116, 223-239.

[Downloaded from pga.iust.ac.ir on 2026-10-19]

[DOI: 10.22068/ijmse.4140]

[20] Chang, S. C., Lin, J. Y., Lu, Y. F., Yeh, J. W., & Shun, T. T. (2021). Thermal spray high-entropy alloy coatings: A review. Journal of Alloys and Compounds, 856, 157297.
[21] Slone, C. E., Zhai, X., & Zhang, Y. (2018). Processing of high-entropy alloys by conventional melting techniques. Materials Characterization, 142, 19-33.
[22] Zhang, Y., Wang, P., & Liaw, P. K. (2018). Mechanical properties of high-entropy alloys: A review. Journal of Materials Research, 33(20), 3290-3306.
[23] Li, Z., Guo, S., & Li, J. (2020). Microstructure and mechanical properties of as-cast high-entropy alloys: A review. Journal of Alloys and Compounds, 814, 152220.
[24] Wen, H., Lavernia, E. J., & Zhang, Y. (2015). Processing high-entropy alloys by severe plastic deformation: A review. Journal of Materials Research, 30(15), 2335-2357.
[25] Liu, B., Wang, Y., & Zuo, L. (2019). Grain refinement and mechanical properties of high-entropy alloys by severe plastic deformation. Materials Science and Engineering: A, 740-741, 19-35.
[26] Zhu, Y., Li, S., & Liaw, P. K. (2021). Post-annealing effects on the microstructure and mechanical properties of high-entropy alloys. Materials Characterization, 172, 110860.
[27] Zhang, Y., Ma, Y., & Liaw, P. K. (2019). Spark plasma sintering of high-entropy alloys: A review. Journal of Materials Research, 34(15), 2533-2549.
[28] Fan, H., Li, G., & Liaw, P. K. (2020). Powder metallurgy of high-entropy alloys. Materials Today Communications, 24, 101297.
[29] Chen, C., Huang, Y., & Liu, Y. (2021). Mechanical alloying and spark plasma sintering of high-entropy alloys: A review. Journal of Alloys and Compounds, 876, 160100.
[30] Tang, H., Liu, W., & Xie, G. (2022). Advances in spark plasma sintering of high-entropy alloys. Materials Research Letters, 10(2), 112-127.
[31] Gao, K., Zhang, Q., & Zhang, H. (2018). Nanostructured high-entropy alloys by powder metallurgy: A review. Materials Science and Engineering: R: Reports, 131, 1-38.
[32] Wei, P., Zhang, J., & Zhang, L. (2019). Ultrafine-grained high-entropy alloys: Processing, microstructure, and mechanical properties. Journal of Alloys and Compounds, 786, 1032-1049.
[33] Ma, S. G., & Li, J. F. (2020). The mechanical properties of nanocrystalline high-entropy alloys. Materials Science and Engineering: A, 785, 139366.
[34] Liu, S., Ma, Y., & Zhang, Y. (2021). Nanostructured CrMnFeCoNi high-entropy alloy synthesized by mechanical alloying and spark plasma sintering: Enhanced strength and ductility. Materials & Design, 203, 109604.
[35] Li, Z., Zhao, Y., & Kou, S. (2019). Microstructure and mechanical properties of CrMnFeCoNi high-entropy alloy prepared by spark plasma sintering. Journal of Materials Science, 54(17), 12102-12112.
[36] Zhang, Y., Gao, H., & Liu, C. T. (2020). Phase formation and microstructure of high-entropy alloys: A review. Materials Characterization, 161, 110168.
[37] Cui, Z., Wang, S., & Zhang, Y. (2022). Microstructural homogeneity and mechanical properties of CrMnFeCoNi high-entropy alloy prepared by different methods. Journal of Alloys and Compounds, 903, 163884.
[38] Ma, Y., Zhang, Y., & Liaw, P. K. (2018). Grain refinement and mechanical properties of high-entropy alloys. Materials Science and Engineering: A, 730, 140-155.
[39] Wang, Q., Li, W., & Wang, Y. D. (2019). Effect of grain size on the mechanical properties of high-entropy alloys. Materials Science and Engineering: A, 755, 163-172.
[40] Singh, P., & Rao, K. P. (2020). Influence of porosity on the mechanical properties of high-entropy alloys. Materials Today: Proceedings, 26, 3719-3724.

[Downloaded from pga.iust.ac.ir on 2026-10-19]

[DOI: 10.22068/ijmse.4140]